AMERICAN
METEOROLOGICAL
SOCIETY

Journal of Atmospheric and Oceanic Technology

EARLY ONLINE RELEASE

The DOI for this manuscript is doi: 10.1175/JTECH-D-17-0196.1

The final published version of this manuscript will replace the preliminary version at the above DOI once it is available.

If you would like to cite this EOR in a separate work, please use the following full citation:

Manić, S., M. Thurai, V. Bringi, and B. Notaroš, 2018: Scattering Calculations for Asymmetric Rain Drops during a Line Convection Event: Comparison with Radar Measurements. J. Atmos. Oceanic Technol. doi:10.1175/JTECH-D-17-0196.1, in press.

Scattering Calculations for Asymmetric Rain Drops during a Line Convection Event: Comparison with Radar Measurements

Sanja B. Manić[1], Merhala Thurai, V. N. Bringi, and Branislav M. Notaroš

Department of Electrical and Computer Engineering

Colorado State University, Fort Collins, Colorado, USA

Submitted to: Journal of Atmospheric and Oceanic Technology

Re-Revised March 2018

[1] Corresponding Author:
Sanja B. Manić
Colorado State University
Department of Electrical and Computer Engineering
1373 Campus Delivery
Fort Collins, CO 80523, USA
Phone: (970) 491- 2967
E-mail: smanic@colostate.edu

ABSTRACT

Two-dimensional video disdrometer (2DVD) data from a line convection rain event are analyzed using the method of moments surface integral equation (MoM-SIE) via drop-by-drop polarimetric scattering calculations at C-band which are compared with radar measurements. Drop geometry of asymmetric drop shapes is reconstructed from 2DVD measurements and the MoM-SIE model is created by meshing the surface of the drop. The Z_{dr} calculations for an example asymmetric drop are validated against an industry standard code solution at C-band, and azimuthal dependence of results is documented. Using the MoM-SIE analysis on 2DVD drop-by-drop data (also referred to as simply MoM-SIE), the radar variables [Z_h, Z_{dr}, K_{dp}, ρ_{hv}] are computed as a function of time (with 1-minute resolution) and compared to C-band radar measurements. The importance of shape variability of asymmetric drops is demonstrated by comparing with the traditional (or, 'bulk') method which uses 1-minute averaged drop size distributions and equilibrium oblate shapes. This was especially pronounced for ρ_{hv} where the MoM-SIE method showed lowered values (dip) during the passage of the line convection consistent with radar measurements, unlike the bulk method. The MoM-SIE calculations of [Z_h, Z_{dr}, K_{dp}] agree very well with the radar measurements whereas LDR calculations from drop-by-drop method are found to be larger than the values from the bulk method which is consistent with the dip in simulated as well as radar-measured ρ_{hv} . Our calculations show the importance of the variance of shapes due to asymmetric drops in the calculation of ρ_{hv} and LDR.

1. Introduction

Polarimetric weather radars make use of the oblate shapes and high degree of orientation of raindrops in order to better estimate rainfall rates from the retrieved raindrop size distributions (Seliga and Bringi 1976; 1978). As a first step, they utilize the differential reflectivity (Z_{dr}) along with the conventionally measured co-polar reflectivity (Z_h), to reduce uncertainties in estimating the drop size distribution within the radar pulse volume (Bringi and Chandrasekar 2001).

The equilibrium shapes of raindrops are size dependent (Beard and Chuang 1987) and they are generally approximated by oblate spheroids whose axis ratios (minor to major) decrease monotonically with increasing size. Drops with diameters smaller than 0.8 mm can be considered almost spherical. For larger drops (>2.5 mm) the concept of dynamic equilibrium shape was introduced by Szakáll et al. (2009) to describe the time-averaged axis ratios due to drop oscillations observed in a wind tunnel which was also confirmed using the concept of 'most probable' shapes from 2-D video disdrometer (2DVD; Schönhuber et al. 2008) by Thurai et al. (2009a). It is now well-known that axisymmetric drop oscillations dominate the background state with smaller amplitude mixed oscillation modes that give rise to *asymmetric* shapes (Beard et al. 2010). However, there is no theoretical framework for modeling such *asymmetric* shapes in natural rainfall. Hence, the common approach is to neglect the variance of drop shapes and to relate the mean axis ratio with drop equi-volume diameter (D_{eq}) (Beard and Chuang 1987; Brandes et al. 2004; Thurai et al. 2007).

Asymmetric drops were inferred from 2DVD measurements in a highly-organized line convection rain event described in Thurai et al. (2013). During this event a significant fraction of drops (around 30%) within the line convection were *asymmetric*. Eight individual *asymmetric* drops were chosen from the 2DVD measurements to reconstruct their 3D-shapes

(Thurai et al. 2017) and to determine their individual scattering amplitudes at C-band using the method of moments in the surface integral formulation (MoM-SIE) (Chobanyan et al. 2015). Scattering calculations for the individual asymmetric drops showed that the single particle differential reflectivity (Z_{dr}) values differed from those calculated assuming rotationally symmetric shapes. Differences were also seen in the case of (single particle) specific differential phase (K_{dp} factor) as well as linear depolarization ratio (LDR).

Accurate simulations of radar observables require accounting for variance of drop shapes which requires computation of drop-by-drop scattering amplitudes and integration of the elements of the covariance matrix over a given measurement interval (Bringi and Chandrasekar 2001). The aforementioned line convection event is analyzed in this manner herein using 3D- reconstruction of drop shapes from 2DVD disdrometer data. Radar reflectivity, differential reflectivity, copolar correlation coefficient and specific differential phase are computed with 1-min time resolution and compared to radar measurements extracted over the 2DVD site from the University of Alabama in Huntsville Advanced Radar for Meteorological and Operational Research (ARMOR) C-band radar (see Petersen et al. 2007; Crowe et al. 2012). The radar is 15 km away from the ground instrument site and the height of the resolution volume is around 340 m at the lowest elevation angle of 1.3°. For completeness the linear depolarization ratio is also computed even though the radar is not configured for measuring LDR. The drop-by-drop scattering simulations are compared with the bulk method which refers to the use of the T-matrix scattering code (Barber and Yeh 1975) with input being the 1-minute averaged drop size distributions from 2DVD, the oblate axis ratios from Thurai et al. (2007) with Gaussian canting angle distribution [mean=0°, σ=5°].

This paper is organized as follows. In Section 2, we revisit the methodology used to obtain the scattering results. Section 3 is reserved for the details of raindrop model construction, used as input to the scattering code. In Section 4, for validation purposes, we consider an example of an *asymmetric* drop that is reconstructed from 2DVD measurements (Thurai et al. 2017) and the results obtained by our electromagnetic solver (MoM-SIE) are compared to those using an industry standard software. We then consider, in Section 5, the line convection event and compare radar measurements with scattering simulations using drop-by-drop as well as the bulk method. The paper concludes with a short Discussion and Conclusions section.

2. Methodology: numerical solution

Raindrop scattering calculations assuming oblate (or rotationally symmetric) shapes typically use the T-matrix method (Waterman 1965; Barber and Yeh 1975; Mishchenko et al. 1996) which is widely used by the radar meteorology community (see, also, Chobanyan et al. 2015 and references therein for a review of different scattering methodologies including discrete dipole approximation, surface and volume integral formulations used for precipitation particles).

Scattering calculations are performed herein using a higher order method of moments solution to the electric and magnetic field surface integral equations (MoM-SIE) based on boundary conditions between air and water dielectric at the rain drop surface, S_a, i.e., the continuity of tangential components of total (incident plus scattered) electric/magnetic fields (Notaroš 2008; Djordjević and Notaroš 2004)

In our current work using the MoM-SIE methodology, a geometrical model is obtained by discretization of the raindrop surface using Lagrange-type curved parametric quadrilateral elements of arbitrary orders (Djordjević and Notaroš 2004; Chobanyan et al. 2015). The method directly solves for an approximation of fictitious surface electric and magnetic current densities, $\mathbf{J}_\mathrm{s}$ and $\mathbf{M}_\mathrm{s}$, over the rain drop boundary using hierarchical divergence-conforming polynomial basis functions, defined over quadrilateral elements (Djordjević and Notaroš 2004; Chobanyan et al. 2015).

For a given incident wave, the scattered electric field is represented as the following function of current densities:

$$\mathbf{E}^{\mathrm{scat}}(\mathbf{J}_\mathrm{s},\mathbf{M}_\mathrm{s},\varepsilon) = -\mathrm{j}\omega\mu_0 \int_{S_\mathrm{a}} \left(\mathbf{J}_\mathrm{s} g + k^{-2}\nabla_\mathrm{s}\cdot\mathbf{J}_\mathrm{s}\nabla g\right)\mathrm{d}S_\mathrm{a} + \int_{S_\mathrm{a}} \mathbf{M}_\mathrm{s}\times\nabla g\,\mathrm{d}S_\mathrm{a} \tag{1}$$

where g ($g = \mathrm{e}^{-\mathrm{j}kR}/4\pi R$) and k ($k = \omega\sqrt{\varepsilon\mu_0}$), respectively, are Green's function and wave number for the unbounded medium of parameters $\varepsilon = \varepsilon_\mathrm{r}\varepsilon_0$ and μ_0, with R being the distance of the field point from the source point, $\omega = 2\pi f$ the angular (radian) frequency, and ε_r the dielectric constant of the rain drop (water). Magnetic field is expressed in a similar fashion.

When the distance R in (1) is zero or relatively small, the singular or near-singular terms are extracted and evaluated analytically, and the remaining non-singular integrals are calculated numerically using Gauss-Legendre integration formulas. The final matrix equation is obtained after the Galerkin testing procedure has been applied to boundary condition equations, which assumes another surface integration of the SIEs with testing (weighting) functions being equal to the basis functions.

For verification purposes, another method that utilizes 3-D geometrical discretization is considered and results are presented in terms of single particle dual-polarization scattering for three different frequency bands.

3. Raindrop modelling

Drop shapes recorded by the 2DVD are used for 3D-reconstruction (for D_{eq} > 2 mm) using the algorithm in Schönhuber et al. (2016). Drops with D_{eq} < 2 mm are assumed to have oblate spheroidal shapes with axis ratio as a function of D_{eq} given in (Thurai et al. 2007). The 3D-reconstruction procedure give rises to more significant errors for small drops (due to resolution of 170 μm) and hence the 2 mm threshold was applied. Note also that the larger drops will have more of an effect on Z_{dr} than the small drops.

Details of the 3D-shape reconstruction of each recorded drop from its images from the two orthogonal cameras have been published previously (Schönhuber et al. 2016; Schwinzerl et al., 2015) hence only a brief summary is given here. The 2DVD measures drop contours in two perpendicular planes which can be skewed due to horizontal component of the drop velocity (typical in line scan camera systems). For drops that possess an axis of symmetry, the contours can be deskewed as described in (Schönhuber et al. 2000; Huang et al. 2008); in addition, the horizontal velocity can be estimated. In the Appendix of Thurai et al. (2017), the horizontal drop velocities derived from the deskewing procedure were shown to be in excellent agreement with the independent wind sensor measurements, both in magnitude and in direction. For deskewing *asymmetric* drops the horizontal velocity must be estimated. This is achieved from the drop horizontal velocities estimated from the deskewed symmetric drops closest in time and size to the *asymmetric* drop (see Section IV of Schönhuber et al., 2016). One limitation of this method for *asymmetric* drops relates to the uncertainty in the exact drop horizontal velocity required as input to the deskewing procedure. However, apart from errors due to rapid fluctuations in wind velocities, we expect the reconstructed shapes to be reasonably representative of their true ‘instantaneous’ shapes.

The deskewed contours in the two orthogonal planes are sampled at equidistant values along the vertical axis and four points are obtained at each height (note that for rotationally symmetric drops the thin 'slices' along the vertical axis are elliptical and the 3D shape is based on stacked ellipses). For asymmetric drops, four different ellipse quarters are constructed for each slice having in mind the center point. The points describing the geometry of each slice are obtained by sampling the constructed elliptical quarters in uniform intervals of the azimuth angle. The procedure is repeated for each slice in order to create the 3D-reconstructed drop, an example of which is shown in Fig. 1. In our models, the shapes of the slices are limited to convex shapes, i.e. the center point needs to be inside or part of the circumference.

The model of the drop is created by defining first order (bilinear) quadrilateral elements, each between four points of the geometry (Thurai et al. 2017). To define one element, two points are chosen with the same coordinate value on the z axis and sequential values on the azimuthal coordinate. Two other points are chosen to have the same azimuth angles but different, consecutive z axis values compared to the two already chosen points. After creating all the elements by connecting pairs of points from groups with consecutive values on the z axis, the elements at the top and the bottom of the drop are defined using all four points from the group having the same z axis value, the highest and the lowest, respectively, so the entire surface of the drop is discretized. The order of the basis functions (Djordjević and Notaroš 2004) used for the unknown expansion over the elements was chosen to comply with Klopf et al. (2012).

4. Validation of the MoM-SIE method

The single particle differential reflectivity, Z_{dr} (expressed as a ratio) is given by:

$$Z_{\rm dr} = \frac{|S_{\rm hh}|^2}{|S_{\rm vv}|^2} \qquad (2)$$

where $S_{\rm hh}$ and $S_{\rm vv}$ are the frequency-dependent backscatter amplitudes for horizontal (h) and vertical (v) polarizations. Fig. 2 shows the calculated $Z_{\rm dr}$ for the reconstructed drop in Fig. 1 as a function of the ('look') azimuthal angle ϕ, for S, C, and X bands. In all three cases, the $Z_{\rm dr}$ variation with ϕ is significant, whereas for a rotationally symmetric drop the $Z_{\rm dr}$ is ϕ-independent, with values of 3.0, 3.7, and 3.2 dB, respectively, marked as '+' points. Fig. 2 also shows that C-band variation lies well above the S and X band variations, which can be attributed to this particular drop size (D_{eq} = 4.81 mm) lying in the C-band resonance scattering region (e.g., Carey and Petersen, 2015). The ϕ-angle variation at C-band is also slightly higher than those at S and X bands.

Although Fig. 2 shows a somewhat periodic variation with the ϕ-angle for all three frequency bands, the real and imaginary parts of $S_{\rm hh}$ and $S_{\rm vv}$ do not necessarily show the same trend. As an example, Fig. 3 shows these variations for C-band. The imaginary part of $S_{\rm hh}$ and $S_{\rm vv}$ show non-periodic variations but their amplitudes are considerably lower than the corresponding real parts. It turns out that the $Z_{\rm dr}$ variation is much more governed by the variation in $Re(S_{\rm hh})$ and $Re(S_{\rm vv})$ than by $Im(S_{\rm hh})$ and $Im(S_{\rm vv})$.

By way of verification of the MoM-SIE based scattering amplitude results, another method that uses 3-D discretization, namely, ANSYS HFSS code[2] (industry standard utilizing the volumetric finite element method – FEM, so numerically very different from the MoM-SIE approach), is employed. Results by the FEM (HFSS) with the computational region truncated by means of a perfectly matched layer (PML) are also included in Figs. 3(a) and

[2] See: http://www.ansys.com/products/electronics/ansys-hfss

3(b). As can be seen, the resulting scattering amplitudes are very close to the MoM-SIE based results. MoM-SIE methods are computationally efficient for electromagnetic problems with small volume to surface ratio and when Green's function can be calculated[3]. FEM-based codes are widely used in computational electromagnetics (in industry), but require discretization of the whole 3 dimensional domain as well as region truncation with boundary condition in order to compute far field scattering results that are easily computed by the SIE method.

5. Calculation of radar variables and comparisons with radar measurements

We now consider the rain event which occurred in Huntsville, Alabama on 25 December 2009. This was a wide spread event with an embedded line convection which traversed the disdrometer site (Thurai et al., 2013). The 2DVD measurements for this event showed that a significant fraction of the drops within the line convection (around 30%) did not possess any rotational symmetry axis (i.e., *asymmetric*).

Altogether, 2DVD measurements over a period of 100 minutes were analysed during which there were 114,317 drops recorded by the instrument, out of which 10,233 drops had $D_{eq} \geq 2$ mm. For all the drops with $D_{eq} \geq 2$ mm, the 3D shapes were constructed in the same way as outlined in Thurai et al. (2017), and their individual scattering amplitudes were calculated using the MoM-SIE method. The individual particle Z_{dr} are plotted as time series in Fig. 4 for two values of incident angle. The top two panels show the Z_{dr} for all drops with $D_{eq} \geq 2$ mm for the entire 100-minute period whilst the two lower panels show the same but

[3] See: https://en.wikipedia.org/wiki/Computational_electromagnetics

for the zoomed in time period. In all cases, the drop sizes are color-coded. The variability in Z_{dr} for a given drop size is particularly evident for the large drops (> 4 mm) and further the dependence on the azimuthal angle is also evident. For all drops with D_{eq} < 2 mm, oblate shapes were assumed whose axis ratios were determined using the diameter-dependent relationship given in Eq. (2) of Thurai et al. (2007). For these drops, the individual scattering amplitudes were also computed with the MoM-SIE. The variability of the single particle Z_{dr} during the line convection passage is evident from Fig. 4(c) though some of the variability is due to sampling errors for the larger sizes which are much lower in concentration. With this consideration the variability in single particle Z_{dr} for a given D_{eq} reflects the variance in shapes due, in part, to the *asymmetric* drops. The coefficient of variation of Z_{dr} (expressed as a ratio) for sizes > 3 mm is around 0.5. The coefficient of variation of the "effective" axis ratio is then ≈ 0.2 using the approximate formula from Jameson (1983). The deduced axis ratio variability is around twice that found by Thurai et al. (2009a) due to *asymmetric* drops.

From the backscatter amplitudes of each individual drop over a finite time period (1-minute) and drop-by-drop integration of the relevant covariance matrix elements (Bringi and Chandrasekar 2001), the radar reflectivity for horizontal polarization (Z_h), differential reflectivity (Z_{dr}) and copolar correlation coefficient (ρ_{hv}) were computed, for comparisons with the C-band ARMOR radar measurements (see Eqs. 3-6, later in the text). This method will also be referred to as the MoM-SIE. Note that for K_{dp} calculation the forward scatter amplitudes are used. The finite time period chosen here is 1-minute, since for smaller averaging period, the sampling errors will be large (Schuur et al. 2001) and for larger averaging period, drop sorting errors will also be large (Lee and Zawadzki 2005). Note from Fig. 4 (c) and (d) that the line convection passage over the disdrometer site took around 15 minutes, from 03:33 UTC to 03:48 UTC.

Fig. 5 shows the PPI (plan position indicator) scan taken with the ARMOR radar (Petersen et al. 2007) at an elevation angle of 1.3 deg. The time of the scan was 03:40 UTC. The 'star' mark represents the location of the 2DVD, and at this time the line convection was directly positioned over the disdrometer site. Panels (a) and (b) show the copolar reflectivity and the differential reflectivity after correcting for attenuation and differential attenuation, respectively. The correction procedures use the specific differential propagation phase based algorithms, using the same procedure described in Bringi et al. (2006). Reflectivity values were high at the site (> 50 dBZ) and differential reflectivity values were also high (> 4 dB) indicating large drops in the strong precipitation shaft. Other PPI scans taken before and after 03:40 UTC can be seen from Fig. 7 in Thurai et al. (2013). Panel (c) shows the corresponding copolar correlation coefficient, ρ_{hv}, and panel (d) marks the areas within the line convection where ρ_{hv} was less than 0.9. Values of attenuation-corrected Z_h and Z_{dr} as well as ρ_{hv} were extracted near and around the radar pixels surrounding the 2DVD site (14.5 km radar range, 52.7 degree azimuth) from all the PPI sweeps that were taken from 03:00 to 04:40 UTC. For a given elevation angle, each sweep was repeated at 5-minute time interval.

The extracted Z_h and Z_{dr} are shown in Figs. 6(a) and 6(b), respectively, for the 100-minute period. For a given PPI sweep time, several points are shown which correspond to the '2DVD-pixel' as well as the 'immediate adjacent' pixels in both azimuth and range, covering approximately an area of 750 m by 750 m over the 2DVD site. Altogether 20 PPI sweeps were used over the entire 100-minute period. Reflectivity and differential reflectivity values reach their highest values at 03:40 UTC. Later on, at around 04:30 UTC, reflectivity values again rise but only up to 40 dBZ. Differential reflectivity remains relatively low, indicating that the maximum drop sizes were significantly lower at 04:30 than at 03:40 UTC. The measured drop size distributions (DSDs) can be seen from Fig. 2(b) in Thurai et al. (2013).

At 03:40, the spectra showed the highest mass-weighted mean diameter and the highest standard deviation of the mass spectrum (not shown).

Over-plotted in black in Figs. 6(a) and 6(b) are the Z_h and Z_dr calculations, based on the individual scattering amplitudes of drops (i.e., drop-by-drop integration using MoM-SIE or simply MoM-SIE) over each 1-minute period. The radar measurements of Z_h and Z_dr show good temporal correlation and agreement with the MoM-SIE as well as bulk calculations with the radar peak values being somewhat larger (60 dBZ and 4 dB) than the simulations perhaps because of disdrometer sampling limitations for large drops or the applied smoothing. While the agreement between MoM-SIE and bulk methods for Z_h is expected, the agreement of Z_dr is somewhat unexpected given the large variance in individual drop Z_dr values in the line convection region (see Fig. 4(c)) especially for the large drops. The bulk method Z_dr is essentially related to the reflectivity-weighted mean axis ratio which would equal the drop-by-drop integrated Z_dr if the axis ratio distribution is narrow (Jameson 1983; Bringi and Chandrasekar 2001). As discussed earlier, the coefficient of variation of the "effective" axis ratio in the line convection is estimated to be around a factor of 2 larger than the value from Thurai et al. (2009a) which is based on data from an artificial rain experiment where *asymmetric* drops were not detected. In spite of this increase, the axis ratio distribution in the line convection case is judged to be narrow enough that the drop-by-drop MoM-SIE computed Z_dr is in good agreement with the bulk method.

Note the radar reflectivity for an individual (i^th) drop, in a volume of 1 m^3, is given by:

$$Z_i = 10^{18} \frac{\lambda^4}{\pi^5 |K_\mathrm{w}|^2} \eta_i \,, \tag{3}$$

where λ is the wavelength in air, $\eta_{\mathrm{h/v}} = 4\pi |S_{\mathrm{hh/vv}}|^2$ is back scatter cross section per unit volume for horizontal/vertical (h/v) polarization, K_w = $(\varepsilon_\mathrm{r}-1)(\varepsilon_\mathrm{r}+2)^{-1}$ = 0.9631–j0.0111 is the dielectric factor of water at C-band with dielectric constant ε_r = 72.5–j22.43. Over a 1-minute period, the resulting reflectivity Z is derived by summing the individual drop reflectivities and is calculated using:

$$Z = \frac{1}{A\Delta t}\sum_i v_i^{-1} Z_i \ , \tag{4}$$

where A is the measurement area of the 2DVD, Δt is the averaging time period, and v_i is the vertical velocity of the i^{th} drop. Equations (3) and (4) are used to evaluate the overall radar reflectivity based on the individual scattering amplitudes for each of the reconstructed rain drops as well as their individual measured fall velocities. The computed Z values for h and v polarizations are converted to the conventional dBZ units and the Z_{dr} in dB is obtained from the difference between the two.

Fig. 6(c) shows the calculated ρ_{hv} values using:

$$\rho_{\text{hv}} = \frac{\left|\sum_i v_i^{-1} S_{\text{hh}}^{*} S_{\text{vv}}\right|}{\sqrt{\sum_i v_i^{-1}\left|S_{\text{hh}}\right|^2 \sum_i v_i^{-1}\left|S_{\text{vv}}\right|^2}} \ , \tag{5}$$

where v_i is the vertical velocity of the i^{th} drop, S represents single drop back-scattering amplitude, and the summation is done over all the drops recorded by the 2DVD during the considered time interval. From 03:35 to 03:40 UTC, a sharp decrease or dip in ρ_{hv} is seen, reaching as low as 0.8. Such low values are consistent with the radar measurement of ρ_{hv} as low as 0.85 in the PPI plot in Fig. 5(d). For comparison, C-band scattering calculations using the 1-minute averaged DSDs and bulk assumptions are included in magenta in Fig. 6(c). The lowest value using the bulk assumptions is only 0.96. Clearly, the drop-by-drop MoM-SIE based calculations give rise to much more accurate ρ_{hv} predictions than the bulk method. This is due to the inability of the bulk method to capture the variability of drop shapes during the line convection passage. Note however, that at other times, i.e., prior to 03:35 UTC and after 03:45 UTC, both methods predict ρ_{hv} values that are close to 1. These values are consistent with radar measurements over the 2DVD site at these other times. The measurement accuracy of ρ_{hv} is around 1% which is substantially less than the simulated change from 0.96 to 0.8-0.85 so the dip should be detectable if the SNR>20 dB or so (Bringi and Chandrasekar 2001).

Figure 6(d) compares the specific differential propagation phase (K_{dp}) derived from the ARMOR range profiles of differential phase (Φ_{dp}) with the corresponding scattering calculations. For the radar-based K_{dp} values, the finite impulse response (FIR) range filtering technique is used, as described in Hubbert and Bringi (1995), having the advantage of quantifying and removing any backscatter differential phase contribution, which at C-band can become significant when large drops or small melting hail are present in the radar pulse volume. However, close examination of the phase data showed the backscatter differential phase $\delta < 3\text{-}5°$ along the line convection which discounts the presence of small melting hail for which δ could reach 20° (Meischner et al. 1991). For the scattering calculations, as in other panels of Fig. 6, the bulk calculations (assuming rotational symmetry) are shown in magenta and the MoM-SIE calculations are shown as black line. K_{dp} is calculated from:

$$K_{\mathrm{dp}} = 10^3 \lambda \frac{180}{\pi} \frac{1}{A\Delta t} \sum_i v_i^{-1} \operatorname{Re}\left[S_{\mathrm{hh}} - S_{\mathrm{vv}}\right], \tag{6}$$

where S represents forward scattering amplitudes. The summation is done over all drops recorded in the considered time interval. The bulk calculations are in good agreement with the MoM-SIE calculations which indicates that K_{dp} is not dependent on the variance of shapes, rather it is related to the mass-weighted mean axis ratio (Jameson 1985; Bringi and Chandrasekar 2001). The radar estimate of K_{dp} is smaller than the calculations due to the range filtering and smoothing methodology used across the compact line convection region.

In Thurai et al. (2017), the cross-polar backscatter from *asymmetric* drops in terms of single-particle (LDR) was also considered. Here we extend to drop-by-drop MoM-SIE LDR calculations as the ratio of the cross-polar reflectivity to the copolar reflectivity and compare that with the bulk method as shown in Fig. 7. It is immediately clear that during the line convection passage, the MoM-SIE method shows much larger LDR than the bulk method (peak of -17 dB versus -26 dB). Even outside the line convection, the MoM-SIE LDR is larger by 3-5 dB relative to the bulk method. We do not have radar data to compare against as the ARMOR radar is not configured for cross-polar reflectivity measurement. However, it is possible to use an analytical equation relating LDR, Z_{dr}, ρ_{hv}, δ and standard deviation of the canting angle (σ_β) (Jameson 1987) to illustrate the consistency between the dip in ρ_{hv} and the peak in LDR from MoM-SIE calculations during the line convection passage. Using Eq. (3.232) from Bringi and Chandrasekar (2001) and setting the values of Z_{dr}=3 dB, ρ_{hv}=0.8, δ=5°and σ_β=10° predicts LDR of -19 dB which is consistent with MoM-SIE peak LDR of -17 dB coinciding with dip in ρ_{hv} to 0.82 (close to radar measured dip of 0.8). On the other hand under the same conditions, setting LDR in Eq. (3.232) to the bulk peak value of -26 dB predicts a much larger ρ_{hv}=0.97 (the dip in bulk ρ_{hv} is only to 0.96). Thus, assuming that the radar measured dip in ρ_{hv} to 0.8 is accurate, we can infer that the MoM-SIE calculated LDR peak of -17 dB is more consistent with radar dip in ρ_{hv} than the bulk peak of -25 dB. It follows that the large MoM-SIE LDR values in the line convection are due to enhanced variance in drop shapes due to presence of *asymmetric* drops which cannot be modelled using the bulk method. Over the entire 100-minute event, Table 1 shows the relative frequency of occurrence of MoM-SIE and bulk LDR values in 5 dB bins. The modal value (at bin center) of LDR for MoM-SIE and bulk method are, respectively, -37.5 and -32.5 dB with the MoM-SIE showing positive skewness.

It should also be noted that because the scattering amplitudes for *asymmetric* drops exhibit ϕ dependence, as we saw earlier in Fig. 3, it is necessary to choose the correct ϕ angle, particularly for the Z_{dr} calculations. In our case, the azimuth angle from the radar to the 2DVD site was 52 degrees, and our reconstruction of drops is referenced to the true North (since the 2DVD was aligned in such a way that this criterion was met), hence we chose the same value for ϕ. In Fig. 8, we compare the single particle Z_{dr} for ϕ = 50, 110, and 180 degrees. Also shown is the [1:1] line. As seen the correlation is high with negligible bias in both plots and as a result any significant ϕ dependence would not be expected when the overall Z_{dr} is calculated for all drops over a 1-minute integration period.

A limitation of the drop reconstruction procedure is that for a given z = *constant* plane, there are only four points available from the two orthogonal cameras, and the 4-ellipse quarters constructed in this plane can have uncertainties in-between these four points. However, because rain drops do not have sharp discontinuities (unlike snow particles), and further they are homogeneous, the resulting errors in the corresponding scattering calculations are not likely to be significant. Another limitation is that deskewing *asymmetric* drop shapes relies on the accuracy of estimating the horizontal drop speed and direction. In the future we will evaluate if the wind speed and direction measured at the height of the 2DVD sensor area can be used to deskew asymmetric drops.

Another possible source of errors when comparing disdrometer-based estimates against radar measurements is the different spatial scales of the radar and ‘point’ 2DVD measurements as well as the height of the radar pulse volume above the surface (340 m in our case). At short ranges considered herein (15 km) the temporal decorrelation between radar and 2DVD is likely to be constrained as evident in Fig. 6. It is well-known that surface point measurements cannot be representative of the radar pixel which is often quantified in terms of point-to-area variance (Ciach and Krajewski 1999; Thurai et al. 2012) which depends on the spatial correlation function of the observable used in the comparison. Other sources of errors include radar-measurement errors and disdrometer-sampling errors. However, it is beyond the scope of this paper to quantify the error variances arising from such error sources (we refer to Thurai et al. 2012 for variance analysis using ARMOR and 2DVD data).

6. Discussion and Conclusions

The bulk method of simulating radar observables such as [Z_h, Z_{dr}, K_{dp}, ρ_{hv}, LDR] in rain involves simplifying assumptions, the main one being related to neglecting the effect of variance in shapes due to presence of *asymmetric drops*, if in fact they occur in significant proportion to the more ubiquitous equilibrium (axisymmetric) shapes. There are very few computations of radar observables that explicitly account for variance in drop shapes. Keat et al. (2016) used the data from an artificial rain experiment reported in Thurai and Bringi (2005) to simulate steady state axisymmetric drop oscillations (assuming Gaussian axis ratio *pdf*) and its effects on ρ_{hv} and Z_{dr} using gamma distribution of drop sizes (DSD) and Rayleigh-Gans theory. Their goal was to retrieve the shape parameter μ of the gamma DSD from radar measurements of [ρ_{hv}; Z_{dr}]. Their bulk simulations indicated drop oscillations had to be taken into account in order for the radar-based retrieval of μ to be unbiased. Thurai et al (2009b) used 2DVD measurements to simulate drop-by-drop scattering but assumed symmetric shapes and canting angles derived from the deskewing procedure as in Huang et al. (2008). The agreement with ARMOR radar measurements was good but they found significant differences in Z_{dr} and ρ_{hv} when compared with bulk methods in one convective rain event.

To the best of our knowledge this study is the first polarimetric scattering analysis of a line convection rain event based on drop-by-drop scattering computations by means of a higher order method of moments in a surface integral equation formulation**,** with *asymmetric* drop geometries being reconstructed from 2DVD measurements. We have compared MoM-SIE surface model discretization results for an example asymmetric drop with equi-volume drop diameter D_{eq}=4.81 mm (in Fig. 1) at S, C, and X bands with volumetric discretization results by an industry standard finite element method based code (HFSS), showing excellent agreement between two methods. The single particle Z_{dr} values showed variability during the passage of the line convection over the 2DVD site with coefficient of variation (when Z_{dr} is expressed as a ratio) of around 0.5 (for drops > 3 mm) which confirms that the variance of drop shapes due to asymmetric drops can be an important factor in this particular case. Note that before and after passage of the line convection the shape variability was sharply reduced.

Drop-by-drop scattering calculations based on 1-minute integration of the covariance matrix elements were performed for the 100-minute event passage over the 2DVD site using the MoM-SIE and the bulk methods. The simulated radar observables were compared with ARMOR radar data extracted from range gates surrounding the 2DVD location. The Z_h, Z_{dr} and K_{dp} were found to be in good agreement between the MoM-SIE, the bulk calculations and the extracted ARMOR data during the line convection passage as well as before and after the passage. However, the bulk method could not simulate the significant lowering of ρ_{hv} during the line convection with dip to 0.8 as measured by radar. The MoM-SIE calculations were able to simulate the dip to 0.8 indicating that the lowered values were a result of variance in shapes due to asymmetric drops. The radar differential phase data showed no evidence of backscatter differential phase (estimated δ < 3-5°) within the line convection and neither did the single drop MoM-SIE calculations ($\delta < 5°$), so this effect could not have contributed to the lowering of ρ_{hv}.

We also computed LDR using drop-by-drop MoM-SIE and the bulk method. During the line convection passage over the 2DVD the MoM-SIE LDR values peaked to -17 dB whereas the bulk LDR was around 8 dB lower (-25 dB). Examination of an analytic expression relating the polarimetric variables showed that the MoM-SIE LDR peak of -17 dB was consistent with the dip in ρ_{hv} to 0.8 (the latter in agreement with the radar observed dip). However, the bulk LDR of -25 dB was not consistent with the observed ρ_{hv} dip, the analytic expression giving a much higher ρ_{hv} value of 0.97 consistent with the calculated bulk value of 0.96. Since the ARMOR radar was not configured for LDR measurements we could not compare with the simulated values. Over the full 100-minute event the modal MoM-SIE LDR values were around -32 .5 dB whereas it was around -37.5 dB for the bulk method. Radars with modest dual-polarized antenna with a system LDR limit of -25 dB (e.g., phased-array airborne radars) could easily detect the LDR peak of -17 dB. However, to detect LDR of -32.5 dB a well-designed antenna capable of system LDR limit of -36 dB would be required (the UK C-band operational radars approach the -36 dB system limit and they routinely measure LDR to detect wet snow aloft; Sandford et al. 2017).

As has been mentioned in earlier publications (Thurai et al., 2013; 2014), 2DVD data examined during most of the rain events showed that the drop shapes conform to the 'most probable' shapes arising from the steady state axisymmetric oscillation mode which can be regarded as the background state. *Asymmetric* shapes occur when the background state is perturbed due to transverse or horizontal modes mixed in which is termed as mixed-mode oscillations (Beard et al. 2010). The line convection system considered here is one of the few exceptions where a significant proportion (≈30%) of *asymmetric* drops was only detected within the line convection but not outside it. Currently, there is no theoretical framework to identify the conditions under which mixed mode oscillations may occur in a persistent manner. For now we have to rely on 2DVD data to first detect the presence of a significant proportion of asymmetric drops in the rain shaft and subsequently to evaluate the conditions under which deviations from the 'most probable' axisymmetric drop shapes occur. Based on this study the most impact would be on quantitative use of ρ_{hv} and LDR with much less impact on Z_{dr} and negligible impact on Z_h and K_{dp}.

Acknowledgements

This work was supported by the National Science Foundation under grant AGS-1431127. We also acknowledge the University of Alabama in Huntsville for providing the ARMOR radar observations used in this NSF study.

The 2DVD data (in the form hyd/hd files) used in this study can be made available upon request from Dr. M. Thurai (email: merhala@colostate.edu), or Dr. P. N Gatlin (email: patrick.gatlin@nasa.gov) or Dr. M. Schönhuber (email: michael.schoenhuber@joanneum.at). ARMOR radar data are archived at University of Alabama @ Huntsville, and can be also made available.

References

ANSYS, High Frequency Structural Simulator (HFSS), Finite Element Method (FEM). http://www.ansys.com/products/electronics/ansys-hfss.

Barber, P., and C. Yeh, 1975: Scattering of electromagnetic waves by arbitrarily shaped dielectric bodies. *Appl. Opt.*, **14**, 2864–2872.

Beard, K. V., and C. Chuang, 1987: A new model for the equilibrium shape of raindrops. *J. Atmos. Sci.*, **44**, 1509–1524.

Beard, K.V., V.N. Bringi, M. Thurai, 2010: A new understanding of raindrop shape, *Atmospheric Research*, **97**, 396-415.

Brandes, E. A., G. Zhang, and J. Vivekanandan, 2004: Drop Size Distribution Retrieval with Polarimetric Radar: Model and Application. *J. Appl. Meteor.*, **43**, 461–475.

Bringi, V. N., and V. Chandrasekar, 2001: *Polarimetric Doppler Weather Radar: Principles and Applications*, Cambridge U. K., Cambridge University Press, 636 pp.

Bringi, V. N., M. Thurai, K. Nakagawa, G. J. Huang, T. Kobayashi, A. Adachi, H. Hanado, and S. Sekizawa, 2006: Rainfall estimation from C-band polarimetric radar in Okinawa, Japan: Comparisons with 2D-video disdrometer and 400 MHz wind profiler. *J. Meteor. Soc. Japan.*, **84**, 705–724.

Carey, L. D., and W. A. Petersen, 2015: Sensitivity of C-band polarimetric radar–based drop size estimates to maximum diameter. *J. Appl. Meteor. Climatol*., **54**, 1352–1371.

Chobanyan, E., N. J. Šekeljić, A. B. Manić, M. M. Ilić, V. N. Bringi, and B. M. Notaroš, 2015: Efficient and Accurate Computational Electromagnetics Approach to Precipitation Particle Scattering Analysis Based on Higher-Order Method of Moments Integral Equation Modeling. *J. Atmos. Oceanic Technol.*, **32**, 1745–1758.

Ciach, G. J., and W. F. Krajewski, 1999: On the estimation of radar rainfall error variance. *Adv. Water Resour*., **22**, 585–595.

Crowe, C.C., C.J. Schultz, M.R. Kumjian, L.D. Carey, and W.A. Petersen, 2012: Use of dual-polarization signatures in diagnosing tornadic potential, *Electronic Journal of Operational Meteor.*, **13**, 57-78.

Djordjević, M. and B. M. Notaroš, 2004: Double higher order method of moments for surface integral equation modeling of metallic and dielectric antennas and scatterers, *IEEE Transactions on Antennas and Propagation*, **52**, 2118-2129.

Hubbert, J., and V. N. Bringi, 1995: An iterative filtering technique for the analysis of copolar differential phase and dual-frequency radar measurements. *J. Atmos. Oceanic Technol.*, **12**, 643–648.

Huang, G., V.N. Bringi, and M. Thurai, 2008: Orientation Angle Distributions of Drops after an 80-m Fall Using a 2D Video Disdrometer. *J. Atmos. Oceanic Technol.,* **25**, 1717–1723.

Jameson, A.R., 1983: Microphysical Interpretation of Multi-Parameter Radar Measurements in Rain. Part I: Interpretation of Polarization Measurements and Estimation of Raindrop Shapes. *J. Atmos. Sci.,* **40**, 1792–1802.

Jameson, A.R., 1985: Microphysical Interpretation of Multiparameter Radar Measurements in Rain. Part III: Interpretation and Measurement of Propagation Differential Phase Shift between Orthogonal Linear Polarizations. *J. Atmos. Sci.,* **42**, 607–614.

Jameson, A.R., 1987: Relations Among Linear and Circulur Polarization Parameters Measured in Canted Hydrometeors. *J. Atmos. Oceanic Technol.,* **4**, 634–646.

Keat, W.J., C.D. Westbrook, and A.J. Illingworth, 2016: High-Precision Measurements of the Copolar Correlation Coefficient: Non-Gaussian Errors and Retrieval of the Dispersion Parameter μ in Rainfall. *J. Appl. Meteor. Climatol.,* **55**, 1615–1632.

Klopf, E. M., N. J. Sekeljić, M. M. Ilić, and B. M. Notaroš, 2012: Optimal modeling parameters for higher order MoM-SIE and FEM-MoM electromagnetic simulations. *IEEE Transactions on* Antennas *and Propagation*, **60**, 2790–2801.

Lee, G.W., and I. Zawadzki, 2005: Variability of drop size distributions: Noise and Noise filtering in Disdrometric data. *J. Appl. Meteor.*, **44**, 634–652.

Meischner, P.F., V.N. Bringi, D. Heimann, and H. Höller, 1991: A Squall Line in Southern Germany: Kinematics and Precipitation Formation as Deduced by Advanced Polarimetric and Doppler Radar Measurements. *Mon. Wea. Rev.,* **119**, 678–701.

Mishchenko, M. I., L. D. Travis, and D. W. Mackowski, 1996: T-matrix computations of light scattering by nonspherical particles: A review, *J. Quant. Spectrosc. Radiat. Transfer*, **55**, 535-575.

Notaroš B. M., 2008: Higher Order Frequency-Domain Computational Electromagnetics. *IEEE Transactions on Antennas and Propagation*, **56**, 8, 2251-2276.

Petersen, W. A., K. R. Knupp, D. J. Cecil, and J. R. Mecikalski, 2007: The University of Alabama Huntsville THOR Center instrumentation: Research and operational collaboration, *Preprints, 33rd Int. AMS Conf. on Radar Meteorology*, Cairns, Australia. [Available online at https://ams.confex.com/ams/33Radar/webprogram/Paper123410.html.]

Sandford, C., A. Illingworth, and R. Thompson, 2017: The Potential Use of the Linear Depolarization Ratio to Distinguish between Convective and Stratiform Rainfall to Improve Radar Rain-Rate Estimates. *J. Appl. Meteor. Climatol.,* **56**, 2927–2940.

Schönhuber, M., W. L. Randeu, H. E. Urban, and J. P. V. Poiares Baptista, 2000: Field measurements of raindrop orientation angles. *Proc. AP2000 Millennium Conf. on Antennas and Propagation,* Davos, Switzerland, IEE, CD-ROM.

Schönhuber, M., G. Lammer, and W. L. Randeu, 2008: The 2D video disdrometer. *Precipitation: Advances in Measurement, Estimation and Prediction,* S. Michaelides, Ed., Springer, 3–31.

Schönhuber, M., M. Schwinzerl and G. Lammer, 2016: 3D Reconstruction of 2DVD-measured Raindrops for Precise Prediction of Propagation Parameters, *10th European Conference on Antennas and Propagation (EuCAP)*, Davos, 2016, pp. 1-4, doi: 10.1109/EuCAP.2016.7481929.

Schuur, T. J., A. V. Ryzhkov, D. S. Zrnić, and M. Schönhuber, 2001: Drop size distributions measured by a 2-D video disdrometer: Comparison with Dual-polarization radar data. *J. Appl. Meteor.*, **40**, 1019-1034.

Schwinzerl, M., M. Schönhuber, G. Lammer, and M. Thurai, 2016: 3D reconstruction of individual raindrops from precise ground-based precipitation measurements. Extended Abstracts, *16th EMS Annual Meeting/11th European Conf. on Applied Climatology*, Trieste, Italy, European Meteorological Society, EMS2016-601. [Presentation available online at: http://presentations.copernicus.org/EMS2016-601_presentation.pptx.]

Seliga, T. A., and V. N. Bringi, 1976: Potential use of radar differential reflectivity measurements at orthogonal polarizations for measuring precipitation. *J. Appl. Meteor.*, **15**, 69-76.

Seliga, T. A., and V. N. Bringi, 1978: Differential reflectivity and differential phase shift: Applications in radar meteorology. *Radio Science*, **13**, 271–275.

Szakáll, M., K. Diehl, S.K. Mitra, and S. Borrmann, 2009: A Wind Tunnel Study on the Shape, Oscillation, and Internal Circulation of Large Raindrops with Sizes between 2.5 and 7.5 mm. *J. Atmos. Sci.*, **66**, 755–765.

Thurai, M., and V. N. Bringi, 2005: Drop axis ratios from a 2D video disdrometer. *J. Atmos. Oceanic Technol.*, **22**, 966–978,

Thurai, M., G. J. Huang, V. N. Bringi, W. L. Randeu, M. Schönhuber, 2007: Drop shapes, model comparisons, and calculations of polarimetric radar parameters in rain. *J. Atmos. Oceanic Technol.*, **24**, 1019−1032.

Thurai, M., V.N. Bringi, M. Szakáll, S.K. Mitra, K.V. Beard, and S. Borrmann, 2009a: Drop Shapes and Axis Ratio Distributions: Comparison between 2D Video Disdrometer and Wind-Tunnel Measurements. *J. Atmos. Oceanic Technol.*, **26**, 1427-1432.

Thurai, M., Bringi, V. N., and W.A. Petersen, 2009b: Rain microstructure retrievals using 2-D video disdrometer and C-band polarimetric radar, *Adv. Geosci*., **20**, 13-18.

Thurai, M., V. N. Bringi, L. D. Carey, P. Gatlin, E. Schultz, and W. A. Petersen, 2012: Estimating the accuracy of polarimetric radar–based retrievals of drop size distribution parameters and rain rate: An application of error variance separation using radar-derived spatial correlations. *J. Hydrometeor*., **13**, 1066–1079.

Thurai, M., V. N. Bringi, W. A. Petersen, P. N. Gatlin, 2013: Drop shapes and fall speeds in rain: two contrasting examples. *J. Appl. Meteor. Climatol.*, **52**, 2567−2581.

Thurai, M., V. N. Bringi, A. B. Manić, N. J. Sekeljić, and B. M. Notaroš, 2014: Investigating rain drop shapes, oscillation modes, and implications for radiowave propagation, *Radio Science*, **49**, 921-932.

Thurai, M., S. Manić, M. Schönhuber, V. N. Bringi, and B. M. Notaroš, 2017: Scattering calculations at C-band for asymmetric raindrops reconstructed from 2D video disdrometer measurements, *J. Atmos. Oceanic Technol.*, **34**, 765–776.

Waterman, P. C., 1965: Matrix formulation of electromagnetic scattering, *Proc. IEEE*, **53**, 805–812.

List of Tables

List of Figures

Figure 1: Reconstructed drop from 2DVD measurements in natural rain (equi-volume drop diameter = 4.81 mm).

Figure 2: Variation of Z_{dr} (in dB) with 'look angle' ϕ, in horizontal plane, for C, S, and X bands shown as dotted lines for the reconstructed drop in Fig. 1. The '+' marks represent the corresponding Z_{dr} values for the most probable shapes.

Figure 3: (a) Real part and (b) imaginary part of C-band back-scatter amplitudes as a function of ϕ, in horizontal plane, for h and v polarizations, for the reconstructed drop given in Fig. 1. Computations using MoM-SIE and HFSS-FEM methods are displayed.

Figure 4: Single particle Z_{dr} for all drops with D_{eq} > 2 mm (a) from 03:00 to 04:40 UTC for ϕ = 50 degrees; (b) the same as (a) but for ϕ = 180 degrees; (c) and (d) are zoomed in versions of (a) and (b) respectively, during the passage of the line convection over the disdrometer site. In all cases, the points are color-coded according to the drop size.

Figure 5: PPI scans of (a) attenuation-corrected Z_h, (b) attenuation-corrected Z_{dr}, and (c) ρ_{hv}, taken at (top to bottom) 03:40 UTC when the line convection was directly above the 2DVD site (marked with an asterisk sign along azimuth 52° and range 15 km). Panel (d) marks the areas within the line convection where ρ_{hv} values were lower than 0.9. :

Figure 6: Polarimetric radar variables comparison between MoM-SIE, bulk method, and radar measurements: (a) Reflectivity (Z_h), (b) Differential reflectivity (Z_{dr}), (c) Copolar correlation coefficient (ρ_{hv}), and (d) Specific differential propagation phase (K_{dp}). The grey line in Fig. 6(d) represents the same MoM-SIE based calculations but with averaging done over a 1-minute time interval rather than 5-minute period.

Figure 7: LDR computation for incident ϕ=50^o and 1 minute averaging.

Figure 8: Single particle Z_{dr} comparison for particles with $D_{eq} \geq 2$ mm for $\phi = 50$ degrees versus $\phi = 180$ degrees (left) and for $\phi = 50$ degrees versus $\phi = 110$ degrees (right). The purple dashed line represents the [1:1] line.

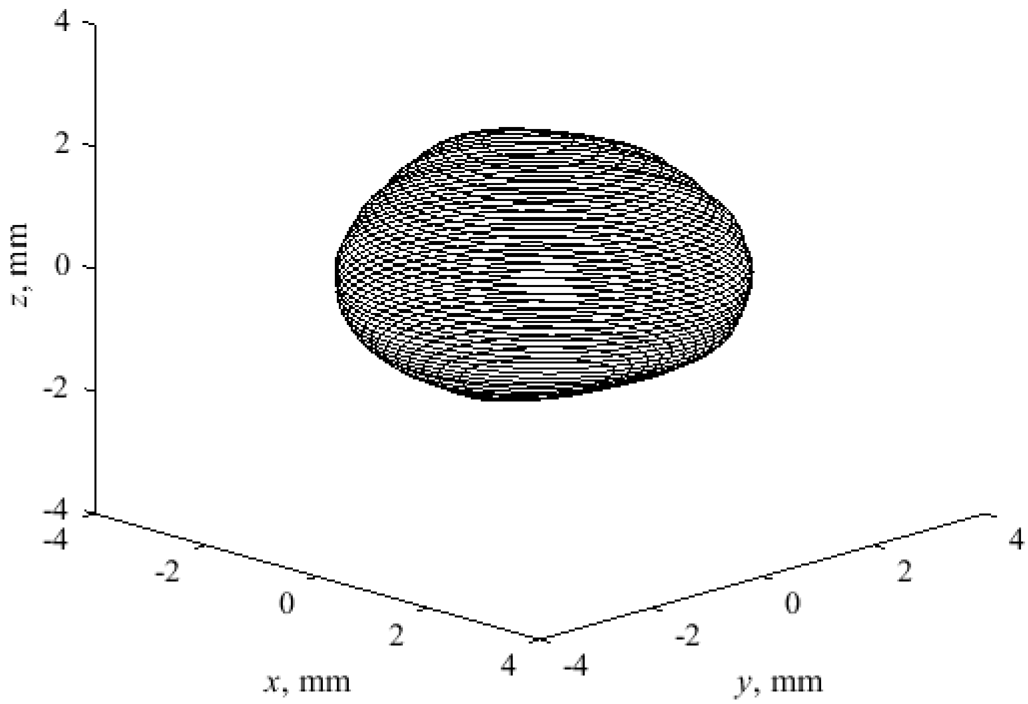

Figure 1: Reconstructed drop from 2DVD measurements in natural rain (equi-volume drop diameter = 4.81 mm).

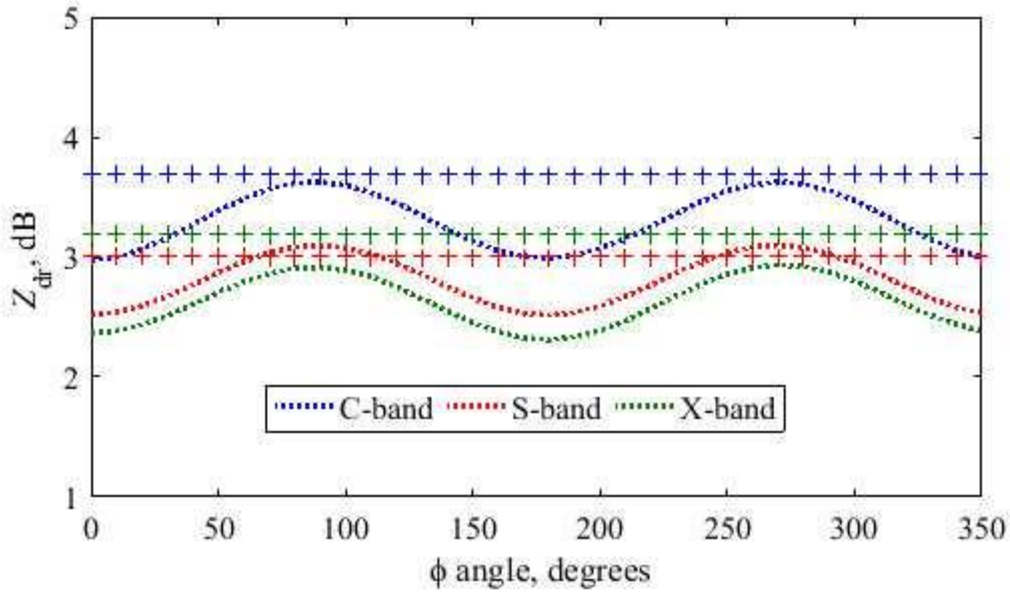

Figure 2: Variation of Z_{dr} (in dB) with 'look angle' ϕ, in horizontal plane, for C, S, and X bands shown as dotted lines for the reconstructed drop in Fig. 1. The '+' marks represent the corresponding Z_{dr} values for the most probable shapes.

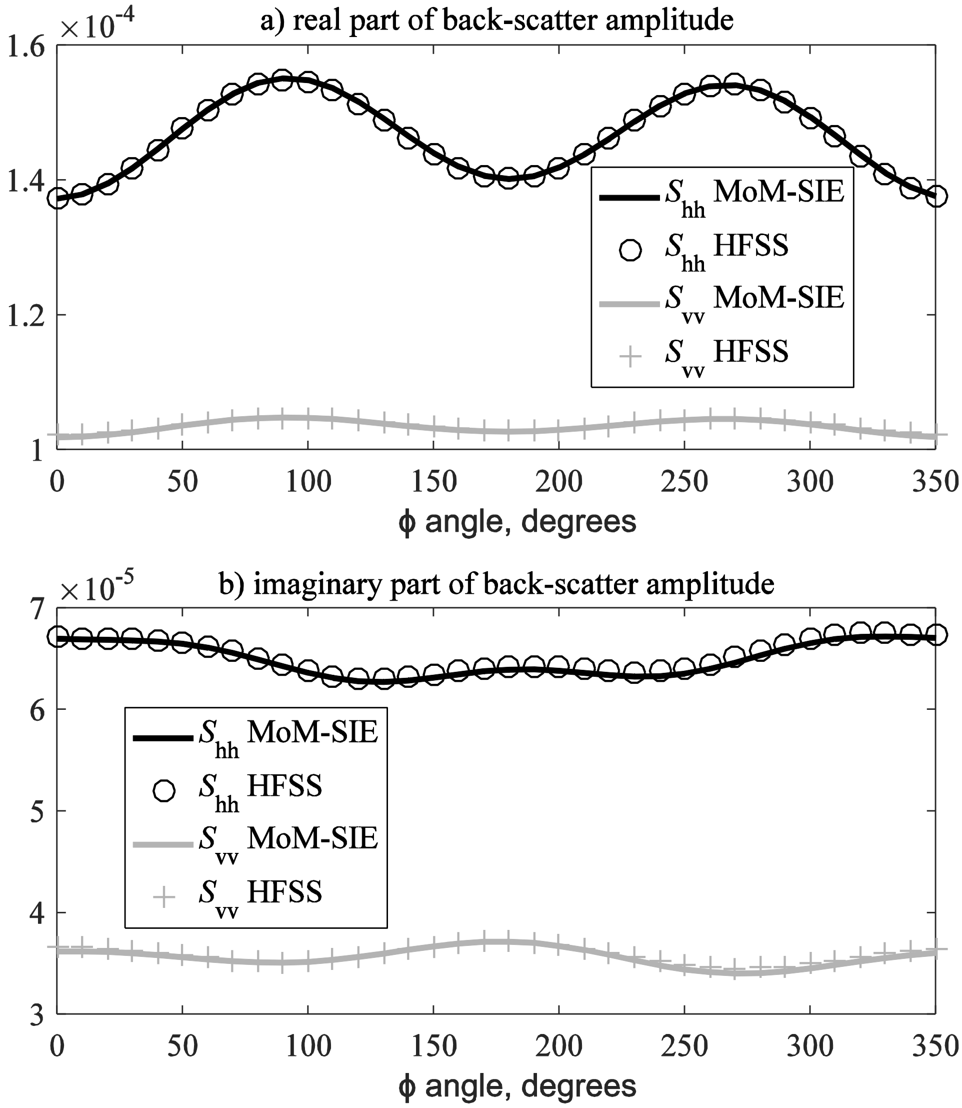

Figure 3: (a) Real part and (b) imaginary part of C-band back-scatter amplitudes as a function of ϕ, in horizontal plane, for h and v polarizations, for the reconstructed drop given in Fig. 1. Computations using MoM-SIE and HFSS-FEM methods are displayed.

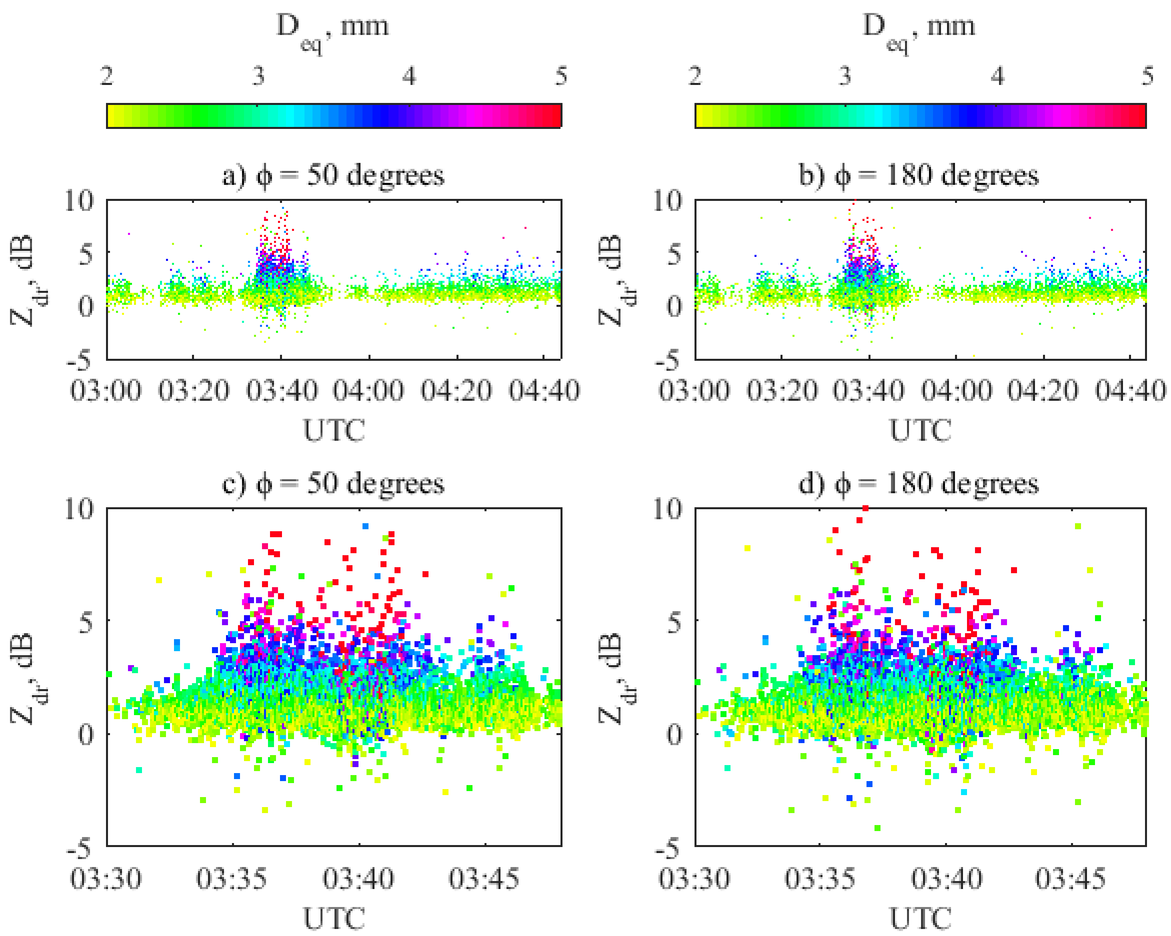

Figure 4: Single particle Z_{dr} for all drops with $D_{eq} > 2$ mm (a) from 03:00 to 04:40 UTC for ϕ = 50 degrees; (b) the same as (a) but for ϕ = 180 degrees; (c) and (d) are zoomed in versions of (a) and (b) respectively, during the passage of the line convection over the disdrometer site. In all cases, the points are color-coded according to the drop size.

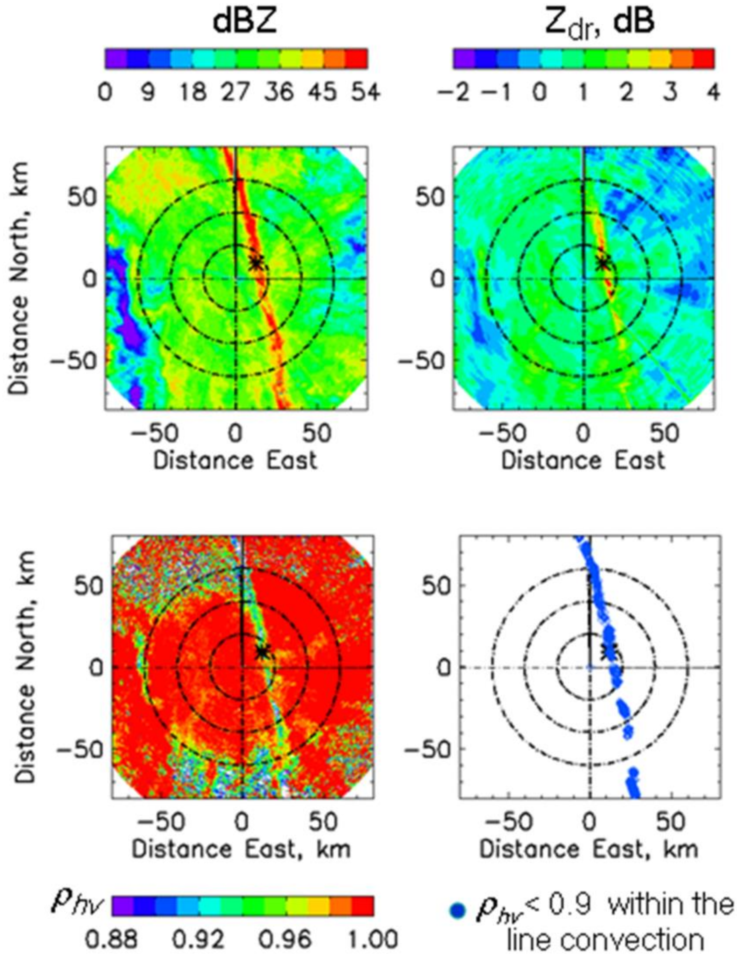

Figure 5: PPI scans of (a) attenuation-corrected Z_h, (b) attenuation-corrected Z_{dr}, and (c) ρ_{hv}, taken at (top to bottom) 03:40 UTC when the line convection was directly above the 2DVD site (marked with an asterisk sign along azimuth 52° and range 15 km). Panel (d) marks the areas within the line convection where ρ_{hv} values were lower than 0.9.

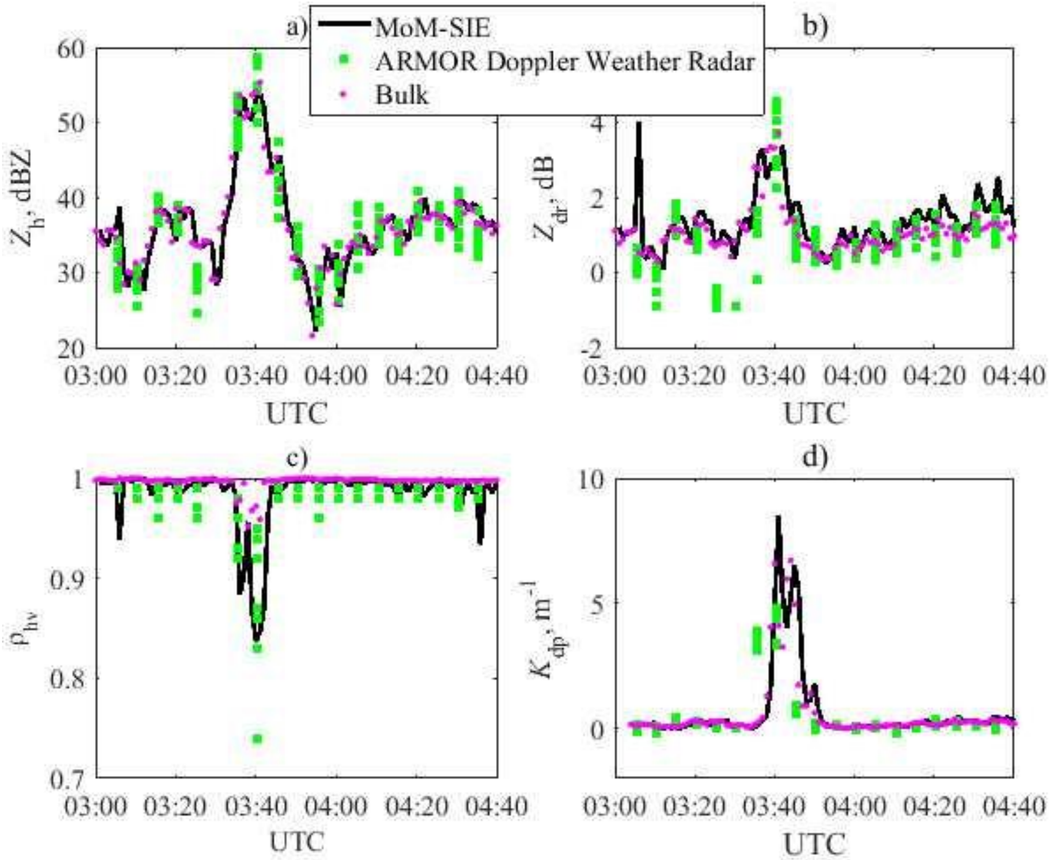

705

706 Figure 6: Polarimetric radar variables comparison between MoM-SIE, bulk method, and
707 radar measurements: (a) Reflectivity (Z_h), (b) Differential reflectivity (Z_{dr}), (c) Copolar
708 correlation coefficient (ρ_{hv}), and (d) Specific differential propagation phase (K_{dp}).

709

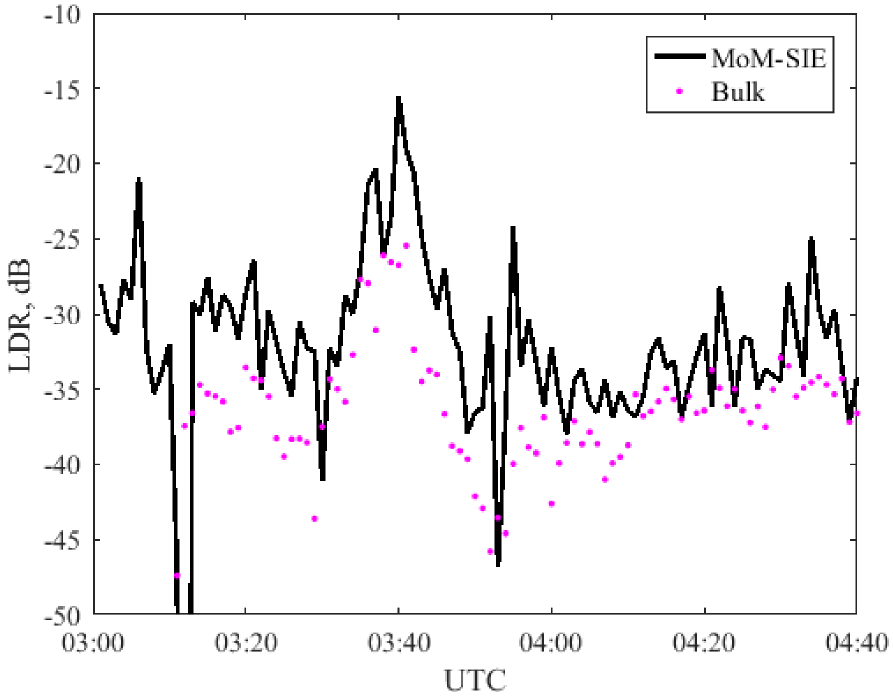

711 Figure 7: LDR computation for incident ϕ=50º and 1 minute averaging.

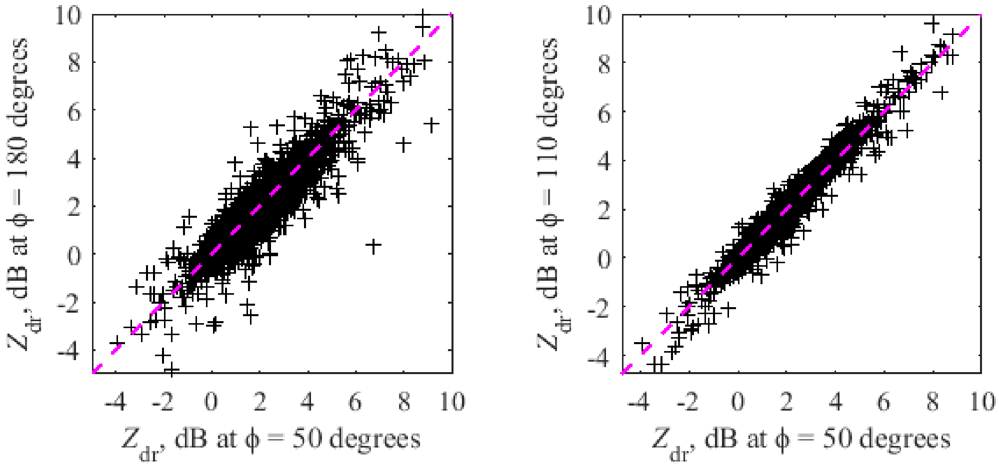

Figure 8: Single particle Z_{dr} comparison for particles with $D_{eq} \geq 2$ mm for ϕ = 50 degrees versus ϕ = 180 degrees (left) and for ϕ = 50 degrees versus ϕ = 110 degrees (right). The purple dashed line represents the [1:1] line.

Table 1

Relative frequency of occurrence (in %) of MoM-SIE and bulk LDR values in 5 dB bins computed with drop-by-drop MoM-SIE and bulk T-matrix methods

Range of LDR, dB	T-matrix	MoM-SIE
< -40	21.3	3.96
-40 to -35	49.2	19.8
-35 to -30	19.7	46.54
-30 to -25	9.8	19.8
-25 to -20	0.0	7.92
-20 to -15	0.0	1.98
-15 to -10	0.0	0
> -10	0.0	0